1991

Forced convective cooling enhancement of electronic package configurations through self-sustained oscillatory flows

Jay S. Nigen
Carnegie Mellon University

Cristina H. Amon

Carnegie Mellon University.Engineering Design Research Center.

Forced Convective Cooling Enhancement *6i* Electronic Package Configurations through Self-Sustained Oscillatory Flows

J.S. Nigen, C.H. Amon

EDRC 24-61-91

Forced Convective Cooling Enhancement of Electronic Package Configurations through Self-Sustained Oscillatory Flows

J. S. Nigen and C.H. Amon
Department of Mechanical Engineering and
Engineering Design Research Center

ABSTRACT

Grooved-channel geometries are formed when electronic components are directly mounted to a substrate. Some grooved-channel geometries have been found to excite and sustain the normally damped instabilities present in Poiseuille flows at lower Reynolds numbers than indicated by linear stability analysis. The resulting self-sustained oscillatory flows improve mixing and thereby enhance convective heat dissipation. Numerical simulations of the flow field and heat transfer characteristics of oscillatory and non-oscillatory flows for five grooved-channel and one suspended block geometry are presented. The extent of heat transfer enhancement is gauged through direct comparison to results corresponding to the steady-flow regime. Local heat transfer coefficients are determined and used to calculate the temperature distribution within a surface-mounted package. Furthermore, the importance of using locally-defined heat transfer coefficients instead of spatially-averaged coefficients for thermal design and analysis is discussed.

This work was supported by the Engineering Design Research Center, a National Science Foundation / Engineering Research Center, under cooperative agreement EDC-8943164 and by the National Science Foundation Grant CTS-8908808.

NOMENCLATURE

a	groove depth (Figure 1)
c	eigenvalue
D	computational domain
h	half-channel height (Figure 1)
K	element number
1	groove width (Figure 1)
L	periodicity length (Figure 1)
Nu	Nusselt number
P	pressure
Pr	Prandtl number
R	Reynolds number
Re	Critical Reynolds number
t	time
T	temperature
T_P	period of self-sustained oscillatory velocity
u,v	velocity components in the x- and y- directions
V	channel-averaged velocity

Greek Symbols

a	streamwise wavenumber
α_{th}	thermal diffusivity
∂D_s	solid wall boundary of D
∂D_p	periodic boundary
\)	kinematic viscosity
II	dynamic pressure
0)	vorticity
o>rs	Tollmien-Schlichting frequency
co	Frequency of self-sustained oscillatory flow

I. INTRODUCTION

The rapid increase in the ability to design and produce chips with high-gate densities has dramatically improved the performance of electronic components. However, increased heat dissipation per unit area is required to maintain acceptable operating temperatures. The well-known exponential relationship between junction temperature and the failure acceleration factor [1] justifies reduction of these temperatures as much as practically and economically possible. Juxtaposed with these reliability issues are market concerns, necessitating that cooling configurations be non-obtrusive to a work environment. Maintenance of an acceptable work environment places restrictions upon the size and acoustic output of any cooling configuration. Such concerns obviously favor natural convection as opposed to forced convection because of the noise produced by a forcing device, (e.g., a fan). Unfortunately, many situations call for more convective heat transport than that possibly rendered through natural convection. The thermal designer must then resort to forced convection and therefore, the addition of a forcing device.

One way to improve convective heat transfer is to diminish the thermal resistance of the boundary layer by reducing its thickness [2]. For turbulent flows, this argument suggests that thermal designers should select a forcing device that produces Reynolds number flows high enough to achieve required convective heat transfer rates. Alternatively, the thickness of the thermal boundary layer may be reduced through surface segmentation. As in the grooved-channel geometry, shown in Figure 1, the thermal boundary layer would have to restart at the beginning of each elevated section. This geometry is naturally present in electronic board configurations with surface mounted components.

An unfortunate consequence of the grooved-channel geometry is the creation of a shear layer between the channel and the groove flows (Figure 2). The shear layer can act as a barrier, reducing or eliminating exchange of fluid between the groove and the channel. In such a case, heat is exchanged between the groove and channel flows mostly through diffusion. Essentially, the fluid in the groove is trapped and merely recirculates, increasing in temperature and diminishing in its ability to remove heat. Many solutions have been proposed which disrupt or remove the shear layer and thereby increase mixing of the fluid. These may be classified as either active or passive techniques.

Active flow destabilization employs external modulation of the flow to disrupt the shear layer and increase communication between the groove and the channel flows [3, 4, 5]. The effectiveness of active destabilization is directly related to the proper selection of the modulation frequency. Alternatively, passive flow destabilization may utilize obstacles, such as cylinders, which are placed in the main flow. These obstacles periodically shed vortices, which serve to disrupt the shear layer and improve mixing [6, 7]. Another passive approach makes use of geometrically induced instabilities to disrupt the shear layer. This is achieved by selecting the flow rate to excite and sustain the normally damped Tollmien-Schlichting waves present in plane Poiseuille flow [8, 9]. The shear layer is disrupted and mixing improved through the interaction of the Tollmien-Schlichting waves in the channel flow with the fluid in the groove. The resulting rates of convective heat transfer are comparable to those of higher Reynolds numbers, namely in the turbulent flow regime. However, the lower velocities serve to reduce acoustic output and the required pumping power [10].

Although all the above methods improve mixing and therefore augment heat removal, the passive methods are perhaps more appropriate to electronic cooling applications because they eliminate the added costs and complexities of an active system [11]. Therefore, an intent of this paper is to demonstrate the effectiveness of passive flow destabilization, through the appropriate selection of the Reynolds number range, in reducing the junction temperature of an example package.

Thermal Design Methodology

The importance of improving product quality and reducing development cycles in today's highly competitive marketplace mandates the use of concurrent design methodology. Concurrent design permits the contributions from different disciplines to be developed in parallel. The high costs and additional time associated with correcting unforeseen flaws, often recognized after production, are thereby reduced. By accounting for thermal considerations concurrently with other design areas, problematic locations can be identified and corrected before physical realization. This economizes the design and production processes while increasing overall confidence in the resultant product.

The analytical techniques used in a concurrent design environment must be independent from physical prototypes. Therefore, numerical approaches are ideally suited and offer added benefit in their ability to isolate individual physical phenomena.

This allows for assessment of particular corrective measures in terms of their possible ramifications upon other aspects of a design. However, the accuracy achieved by a numerical simulation is directly related to the number of degrees of freedom. Therefore, accuracy is achieved only at the cost of time.

A possible solution to this dilemma is to gradually increase the complexity of the simulation with the advance of the design process. In the initial stages of a design, *ballpark figures,* which may be achieved at relatively little cost in time, allow for the evaluation of the general aspects of a design. This period is essential in concurrent design because of the informational overhead required before the initiation of the parallel stage. As the design becomes more specific, additional accuracy can be obtained without hindering the other aspects of the design. This procedure is readily applicable to the thermal design of electronic components.

The major time consumer in a conjugate conduction/convection simulation of an electronic component is the solution of the coupled Navier-Stokes and energy equations for the convecting flow. Their solution is required to determine the behavior and characteristics associated with the surrounding fluid. The solution of the flow field is then used to determine the heat transfer coefficients associated with the environmentally exposed surfaces. In the initial stages, assumed heat transfer coefficients may be used, thus eliminating the need for the fluid solution. This procedure only requires the solution of the heat equation and thereby dramatically reduces the overall time to conduct a simulation. However, the accuracy of the solution is directly related to the suitability of the assumed heat transfer coefficients. Gradually, more complex correlations can be introduced to improve the accuracy of the heat transfer coefficients. The final stage of the concurrent thermal design procedure would include a complete thermal-fluid simulation. This sequence would result in an accurate description of thermal performance without hindering the progress of other design areas.

The mathematical formulation and discretization associated with the numeric simulation method is described in the following sections. The temporal discretization is accomplished using finite differences, while the spatial discretization is conducted using the spectral element technique [12, 13]. The spectral element technique is a high-order, weighted-residual technique that combines the geometric flexibility of the finite element technique with the accuracy and rapid convergence of spectral methods. Using this solution technique, the Navier-Stokes and energy equations are solved to

investigate the forced convective phenomena associated with six geometries. The first three, Groove 1, Groove 2, and Groove 3 differ only in groove width, i.e. separation between components. The next two, Smount 1 and Smount 2, represent surface mounted components with different heights, leading to varying groove depths. The remaining geometry, Ivtpga, is an inverted pin grid array geometry and is selected to explore the possible significance of communication underneath a package. These geometries are studied with the intent of investigating the relationship between the behavior of the fluid and the heat transfer coefficients. Moreover, the significance of specifying a spatially varying heat transfer coefficient will be demonstrated.

II. MATHEMATICAL FORMULATION

The geometric domain to be examined is the grooved-channel geometry (Figure 1), which is periodic in the streamwise direction, x, and infinite in depth, z, rendering the problem two-dimensional. The incoming velocity field is considered to be periodically fully developed and the fluid is assumed to be incompressible with constant properties.

The continuous problem is formulated using the Navier-Stokes equations, and conservation of both mass and energy. The nondimensionalized Navier-Stokes [14], expressed in rotation form, and continuity equations are,

$$3v(x,t)/3t = v(x,t) \times co(x,t) - VI''I(x,t) + R\text{-}^{l}V^{2}v(x,t) \quad \text{in } D \tag{1}$$

$$V\text{-}v(x,t) = 0 \qquad \text{in } D \tag{2}$$

where $co(x,t) = V \times v(x,t)$ is the vorticity, $n(x,t) = p(x,t) + 0.5|v(x,t)|^2$ is the dynamic pressure, $v(x,t) = u\hat{x} + v\hat{y}$, j_S the velocity, $R = 3Vh/2v$ is the Reynolds number, and x and t represent space and time, respectively.

The energy equation is given as

$$9T/9t = (R.Pr)'^{1}\ V^{2}T - V(vT) \qquad \text{in } D \tag{3}$$

where $Pr = v/a_t h$ is the Prandtl number, v and oc_{lh} are the kinematic viscosity and thermal diffusivity of the fluid.

The numerical approach used is that of direct simulation, using initial value solvers.

Additionally, all coupling between the fluid and the heat transfer equations is through the convective terms in (3). In particular, the temperature is passive and does not drive the flow, and the viscous dissipation does not enter as a source term in the energy equation.

III. TEMPORAL DISCRETIZATION

The temporal discretization of the Navier-Stokes equations must accomplish three major objectives. First, limitations in computer time require that the nonlinearities be treated explicitly, that is the convective term should be calculated from values of the velocity from the previous time step. Second, the viscous term should be treated implicitly to avoid having unreasonable time-step restrictions. These time-step restrictions would be prohibitive because of the high resolution of spectral techniques adjacent to boundaries [15]. Third, the dynamic pressure, FI, must be calculated so that the velocity is divergence free. In response to these needs, a three-step, time-splitting scheme for the semi-discrete formulation of the time-dependent term in the Navier-Stokes equation will be used. By treating the non-linear terms explicitly, the complete solution of the Navier-Stokes equations involves first solving a wave-like equation for the nonlinear, convective terms and then elliptic Poisson and Helmholtz equations for the pressure and viscous terms, respectively. This time-splitting scheme has been successfully implemented by other researchers [13, 14].

IV. SPATIAL DISCRETIZATION

The spatial discretization of the domain is obtained with the spectral element method. The domain is decomposed into a series of quadrangular sub-domains or elements which are isoparametrically mapped from the physical into the computational space. A spectral element mesh for a grooved-channel geometry depicting the elemental subdivision is displayed in Figure 3a and including the collocation points in Figure 3b.

The convective step is formulated using a pseudo-spectral or collocation approach. This allows for economical treatment of the nonlinear velocity terms. For the viscous and pressure steps, the discrete equations are generated for each element by inserting the interpolants and the transformed nodal collocation values into the

variationally formulated, weak form of the equation. Then a Galerkin, weighted-residual technique is implemented and the resulting equations are integrated, requiring stationarity at the collocation points.

Once the system of discrete equations is obtained for each element, the global matrix is constructed using *direct stiffness* summation. The spectral solutions are C° across the boundaries of the elements with interfacial continuity constraints imposed through the variational formulation. This alleviates the need for a *patching technique,* usually required to obtain interfacial continuity in multi-domain spectral techniques. Assembly of the global matrix is accomplished using parallel static condensation in which the nodes and their corresponding degrees of freedom are decoupled into those lying on the boundary of elements and those interior to an element. The boundary nodes are determined first by inverting the condensed system, which is of greatly reduced rank, and then, the interior nodes may be determined in parallel, through matrix multiplications.

The inversion of the global system matrix is carried out directly (LDL^T decomposition) in a preprocessing stage at the beginning of a simulation. From then on, only matrix multiplications are performed at each successive time step, resulting in an efficient implementation.

V. LINEAR STABILITY

By assuming that laminar flows are effected by the presence of perturbations, it is possible to formulate a representation for transition in some simple geometries. By doing so, one can follow the behavior of such disturbances and determine whether they decay, grow, or remain fixed in amplitude. An additional assumption is made which consists of prescribing that the magnitude of the characteristics associated with the disturbance are *small.* This enables the elimination of any quadratic combinations of disturbance components [16]. After some manipulation, the resulting expression is the Orr-Sommerfeld equation [17],

$$(iaR)^{-1}(D^2 - a^2)^2 \phi = (U - c)(D^2 - a^2)\,\$ - (D^2U)\langle\rangle \qquad (4)$$

which represents the Navier-Stokes equation linearized about a steady, fully-

developed velocity profile. D refers to differentiation, a is the wave number in the streamwise direction, R is the Reynolds number, U is the steady velocity profile, and ϕ is Fourier series representation of the perturbation.

For any specified values of a and R, there exists a corresponding infinite discrete spectrum of eigenvalues, c, yielding nontrivial solutions. Each eigenfunction has an associated velocity of propagation or phase speed, Real(c), and growth rate, Im(c), respectively. The eigenfunction with the maximum growth rate will physically correspond to the least-stable mode, usually referred to as *Tollmien-Schlichting waves.*

In plane channel flow, the growth rate is found to be negative for Reynolds numbers less than 5772. This indicates that a *small* disturbance introduced into such a flow will decay in time, resulting in parallel flows. In the grooved-channel geometry, the periodic presence of elevated sections will serve to sustain the Tollmien-Schlichting waves, resulting in oscillatory flows. These sustained oscillations occur at lower Reynolds numbers (of the order 0(100)) than indicated by the linear theory for the corresponding plane channel flows.

VI. TIME-PERIODIC FLOWS

According to linear hydrodynamic stability analysis, a critical Reynolds number exists, R_c, beyond which a flow is no longer stable. In the case of grooved-channel geometries, supercritical flows, or flows at Reynolds numbers greater than R_c, exhibit traveling waves in the channel. It has been determined that the amplitude of these waves is proportional to $\overline{R-R_c}$ I[18]-

A complex relationship exists between the traveling waves, present in the channel, and the groove flow. The resulting effect is that the normally stationary vortex within the groove undergoes a repetitive pattern of change. A flow that exhibits these characteristics is considered to be in a *time-periodic state.*

An observed consequence of such a time-periodic pattern is a vast increase in the exchange of fluid between the channel and groove flows. This is apparent by contrasting the steady flow pattern in Figure 2 with the sequence corresponding to a time period of the supercritical flow, as depicted in Figure 4. In the first frame (t=0) of

the sequence portrayed in Figure 4a, the traveling waves are compressing the downstream side of the vortex while allowing the upstream side to expand into the channel. This process serves to coalesce the two vortex structures in the center of the recirculation zone.

In the second frame (t=Tp/5), there exists only one main vortex. However, the channel flow is beginning to separate the vortex and its associated shear layer from the upstream face. In so doing, channel fluid enters and circulates in the groove (third frame, t=2Tp/5) before being evacuated by the main vortex. This process, coupled with the compression caused by contact with the traveling waves, begins to force the main vortex towards the downstream face. This permits more channel flow to enter into the groove.

As depicted in the fourth frame (t=3Tp/5), channel fluid has consumed more than half of the groove. The channel fluid, which is flowing over the upstream face, undergoes separation as in flow over a backstep. This creates another vortex that grows in size and begins to fill the groove. This expansion begins to choke off the supply of channel fluid. Additionally, the traveling waves begin to compress the preexisting, downstream vortex that had expanded into the channel. The expansion of the upstream vortex coupled with the compression of the downstream vortex, forces the two towards each other.

Frame five (t=4Tp/5) clearly shows that the upstream vortex has grown to approximately the same size as the downstream vortex. The traveling waves have fully compressed the downstream vortex, allowing channel fluid to come in direct contact with the downstream corner. However, no channel fluid enters into the groove. This is because the two main vortices are surrounded by a larger, single recirculation zone, which forms a shear layer with the adjacent traveling waves. The outer recirculation zone removes the *driving force* for the upstream vortex by blocking any contact with the channel flow. Frame six ($t=T_p$) demonstrates that the outer recirculation zone has effectively starved the upstream vortex of momentum, forcing it to combine with the downstream vortex. Frame six completes the sequence and initiates the new one.

This cycle repeats in a periodic fashion, allowing for an organized exchange of channel and groove fluid. Additionally, the channel flow does not exhibit the characteristic turbulent velocity profile. This results in less viscous dissipation, leading to lower pumping power requirements for similar heat transfer rates [10].

The same basic characteristics of the repetitive flow sequence demonstrated in Figure 4a are exhibited for other geometries, shown in Figures 4b, c, and d. Namely, the separation phenomena associated with the upstream corner and the movement of the preexisting vortex with respect to the channel waves, dictates the flow in the groove. This would indicate the existence of the same basic flow pattern for the relative dimensions of the geometries studied. The major difference among the six geometries is the amplitude of the traveling waves with respect to Reynolds number. Since unsteadiness leads to better mixing, the desirability of maximum wave amplitude for a given Reynolds number is self evident.

	GROOVE 1	GROOVE 2	GROOVE 3
groove depth, a/h	0.715	0.715	0.715
groove width, l/h	2.500	3.000	2.000
channel height, 2h/h	2.000	2.000	2.000
periodic length, L/h	5.000	5.500	4.500

Table 1. Summary of Geometric Dimensions

To investigate the effect of groove width upon the thermal and fluid performance of a geometry, three cases are analyzed. The first case, Groove 1, has a groove width equal to that of the component width. The second and third cases, Groove 2 and Groove 3, have larger and smaller groove widths, respectively. The distances, non-dimensionalized by half the channel height, are summarized in the Table 1.

Simulations are conducted for each geometry for a subcritical and supercritical Reynolds number i.e., for Reynolds number smaller than and greater than R_c, respectively. To establish a good basis for comparison, the subcritical Reynolds number for all of the Groove cases was selected to be 450, while 375 was selected for the other geometries. The supercritical Reynolds number selected for each case is as follows: 780 for Groove 1, 700 for Groove 2, 930 for Groove 3, and 800 for Smount-1, Smount-2, and Ivtpga. These Reynolds numbers are selected because the resulting flow fields (Figure 5) contain substantial oscillations. However, direct comparisons between each of the supercritical cases must be made with respect to the amplitude of the oscillations, because each has a different critical Reynolds number.

By storing data at a fixed location throughout the simulation, it is possible to construct an oscillogram for the velocity. Subtracting the time-averaged velocity contribution, only the signal corresponding to the oscillatory component of the flow will remain. By taking the discrete Fourier transform of this signal, it is possible to decompose the oscillatory component into its individual Fourier modes. At the critical Reynolds number, the resulting frequencies for the least stable mode, ω, agree well with the frequencies predicted by the linear theory, ω_{rs}. This suggests that the disturbances are Tollmien-Schlichting in nature and that the simulations are accurate. For each Groove geometry, a summary of the critical Reynolds number (± 2 %) and the corresponding frequency of the least stable mode is presented in Table 2.

	GROOVE 1	GROOVE 2	GROOVE 3
Re	595	545	710
ω_{rs}	0.523326	0.460287	0.593866
ω	0.518502	0.476176	0.592575
Error	0.9219%	3.4519%	0.2173%

Table 2. Summary of Critical Reynolds Numbers

Oscillograms for the Groove geometries corresponding to a point located at the center of the main channel and 10% of the distance along the component are displayed in Figure 6a. These oscillograms represent the streamwise u-velocity component as a function of time. Notice the repetitive, steady-periodic nature of the velocity response. Figure 6b indicates the result of a Fourier-power analysis conducted for each of the above signals. Although oscillograms for other points in the channel may result in signals with subharmonics and varying coefficient amplitudes, the same fundamental frequency is present.

In time, only one mode, the least stable mode, will not decay. This remaining mode exhibits a frequency which has shifted from that corresponding to the critical Reynolds number. This is attributable to the nonlinear effects, which are significant for

disturbances with finite amplitudes. Such *finite-amplitude* disturbances have been found to differ in frequency from the value predicted by linear stability theory [14]. However, the traveling wave nature of the instabilities supports the assertion that the channel instabilities are Tollmien-Schlichting waves.

The Smount 1 and Smount 2 geometries were investigated to ascertain the effect of groove depth upon the amplitude of the traveling waves. As indicted in Table 3, the difference in the frequency of oscillations between these two geometries is negligible, demonstrating the dominance of groove length rater than depth upon frequency selection. However, Smount 1, having a 20% deeper groove, exhibits higher amplitude disturbances. This is attributable to the larger portion of the total depth, ie. groove plus channel depth, that the package constitutes in Smount 1.

Interesting, Ivtpga, which has the same groove depth as Smount 1, while having the same package height as Smount 2, exhibits the highest amplitude disturbances. This may be attributable to the momentum contribution of the flow underneath the package. However, the relationship between the groove, channel, and under-package flows is complex and requires more study.

	SMOUNT 1	SMOUNT 2	IVTPGA
CO	0.599259	0.595536	0.586232
Amplitude	5.7211 E-4	4.3289 E-4	6.6555 E-4

Table 3. Summary of Frequency and Amplitude of Oscillations

VII. HEAT TRANSFER ENHANCEMENT

The benefit of increased exchange of fluid between the channel and the groove is self evident by contrasting the stratified isotherms for steady flow (Figure 7a) with those corresponding to periodic oscillatory flow (Figure 7b). These calculations are performed under the assumption of uniform heat flux along the bottom wall and adiabatic conditions along the top.

To represent the extent of cooling enhancement achieved by the oscillations, local heat transfer coefficients are calculated. These results should be applicable to the

case of non-uniform heat fluxes as long as the flow is well mixed. Therefore, the oscillatory case is a better approximation of individual, heat generating packages than the non-oscillatory case.

The local, time-dependent heat transfer coefficients are calculated for each geometry and averaged in time, over one cycle. The results for both the oscillatory and non-oscillatory cases are displayed graphically, as a function of node number, in Figure 8,10, and 11.

A direct relationship becomes apparent by comparing the improvement in the local heat transfer coefficients (Figure 8, 10, and 11) with the amplitude of the oscillations in the velocity (Figure 6). Additionally, the same general pattern of enhancement is present. Namely, in all the geometries, the heat transfer coefficients corresponding to the oscillatory flow improve dramatically at the upstream corner with respect to the steady flow values. A significant improvement is also realized in the upstream groove bottom. Both of these improvements can be attributed to the increase in velocity of the upstream vortex caused by interaction with the traveling waves in the channel. Additionally, the upstream corner's improvement is also related to its direct exposure to the channel flow as previously described. A comparison of the local heat transfer coefficient of each Groove geometry for the non-oscillatory case (R=450) is given in Figure 9. In this case, by increasing the separation between components, convective enhancement is realized. This is a consequence of the vortex structure in the groove flow and availability of more fluid to absorb energy.

VII. SAMPLE PACKAGE

A sample surface-mounted electronic package was constructed to demonstrate the effect of self-sustained oscillatory flows upon the maximum junction temperature. The sample package is based upon a power semiconductor (Harris TO-220), although the heat generation, size, and material properties have been adjusted to those comparable to a small VLSI chip. The spectral element mesh for the sample package is displayed in Figure 12a and with collocation points in Figure 12b, while the general configuration is depicted in Figure 12c. Material properties, summarized in Table 4, were selected to both emphasize improved thermal performance and retain realism. In spite of its handling and manufacturing difficulties, Beryllia is used for both the cap and the substrate because of its promise for use in future packages [19]. A plastic cap

is also used to demonstrate the impact of using a Beryllia cap upon thermal performance. The chip is specified to produce 5.0 x 10^4 W/m^2 of heat flux. Temperature distributions within the sample package are calculated using the time-averaged, locally-varying, heat transfer coefficients. For all cases, the heat transfer coefficient along the bottom of the substrate is specified as 0.5 W/m^2-C. This value corresponds to a natural convective boundary condition.

The isotherms depicted in Figure 13a calculated using the heat transfer coefficients corresponding to the periodic oscillatory case for Groove 3 at R=930. Additionally, the cap is composed of plastic. The maximum temperature is 88.55 C and the minimum is 76.13 C, yielding a temperature range of 12.42 C. The isotherms depicted in Figure 13b correspond to the heat transfer coefficients associated with the steady flow regime at R=450, with a plastic cap. The corresponding maximum temperature is 119.6 C and the minimum is 108.2 C.

The difference in maximum temperatures for the oscillatory and non-oscillatory flow regimes is significant. In fact, for the steady flow regime, the maximum temperature of the component is 35.06% greater than for the oscillatory flow. Additionally, the temperature range experienced by the package differs by 1.02 C for the parallel versus oscillating flow conditions.

Component	Material	Thermal Conductivity Watts/ C • m	Width m	Height m
Substrate	Beryllia	218.0	0.0450	0.0072
Solder	Pb-5%Sn	63.0	0.0225	0.0012
Case	Cu Alloy	264.0	0.0225	0.0072
Chip	Si	147.0	0.0050	0.0012
Cap I	Plastic	0.260	0.0012	0.0012
Cap II	Beryllia	218.0	0.0012	0.0012
Fluid	Air@20°C	2.62E-2	—	—

Table 4. Sample Package Data

In order to emphasize the significance of using Beryllia as an encapsulant, the temperature field within the package was determined under the oscillating flow conditions, with a Beryllia cap. As depicted in Figure 13c, the maximum temperature is 84.90 C and the minimum is 83.71 C. The use of Beryllia in the cap has reduced the maximum temperature by 3.65 C. However, the temperature range existing in the package is only 1.19 C, compared to the 12.42 C for a plastic cap . Reduction in the temperature gradient may result in a significant reduction of the thermally induced stresses sustained inside the package.

Much experimental work has been conducted to determine average heat transfer coefficients [20, 21, 22] for grooved-channel geometries in two and three dimensions. However, use of such spatially-averaged heat transfer coefficients in thermal design can result in significant differences in maximum temperature. As an example, an average heat transfer coefficient corresponding to the oscillating flow field was calculated and used to generate the isotherms in Figure 13d. The cap is specified as consisting of the plastic material. The maximum temperature obtained was 86.35 C. The maximum temperatures obtained with the use of spatially-averaged and locally-varying values differ by 2.48 %. However, the temperature range experienced by the package is 25.64 % less by using spatially-averaged heat transfer coefficients. This difference could have a significant impact in terms of stress predictions within a package.

In the case of surface-mounted components, the highest heat transfer coefficients will exist along the top surface of the chip. Therefore, the accuracy of the spatially-averaged coefficient will be related to the amount of the total perimeter that corresponds to the top surface. In this case, the use of the average value leads to a conservative estimate in terms of maximum temperature, but underestimates the temperature range. However, this may not always be so, suggesting that the thermal designer must be careful when using spatially-averaged values for the heat transfer coefficient.

CONCLUSION

A numerical investigation of the thermal and fluid behavior of five different grooved-channel geometries, three differing only in groove width, two differing only in groove depth, and a suspended block geometry, is conducted. The same basic flow patterns

exist within the grooves for all of the geometries. Likewise, a similar geometric distribution of local heat transfer coefficient magnitudes was found. This pattern would allow for the construction of a *spatial-corrector,* to more accurately account for geometrical variance upon the magnitude of spatially-averaged, heat transfer coefficient correlations.

The effectiveness of self-sustained oscillatory flows in enhancing convective cooling of surface-mounted packages is demonstrated through a comparison of maximum temperatures. Furthermore, it is found that the use of spatially-averaged heat transfer coefficients can lead to significantly different maximum temperatures for a sample package, possibly leading to ineffective thermal design.

REFERENCES

[1] *Handbook for Predictions of Electronic Equipment Reliability,"* U.S.A.F. Rome Air Development Center, 1982.

[2] W.M. Kays and M.E. Crawford, Convective Heat and Mass Transfer. New York, McGraw-Hill Book Company, 1980, p. 207.

[3] I. J. Sobey, "On Flow Through Furrowed Channels. Part 1. Calculated Flow Patterns," J. *Fluid Mech.,* Vol. 96, pp. 1-26, 1980.

[4] N.K. Ghaddar, K.Z. Korczak, B.B. Mikic, and AT. Patera, "Numerical Investigation of Incompressible Flow in Grooved Channels. Part 2. Resonance and Oscillatory Heat-Transfer Enhancement," *J. Fluid Mech.,* Vol. 168, pp. 541-567, 1986.

[5] M. Greiner, "An Experimental Investigation of Resonant Heat Transfer Enhancement in Grooved Channels," to appear in *Int. J. of Heat and Mass Transfer*,1991.

[6] E. Ratts, C.H. Amon, B.B. Mikic, and AT. Patera, "Cooling Enhancement of Forced Convection Air Cooled Chip Array through Flow Modulation Induced by Vortex-Shedding Cylinders in Cross-Flow", Cooling Technology for Electronic

Equipment, ed. W. Aung, New York, Hemisphere Publishing Company, pp.183-194, 1988.

[7] G.E. Kamiadakis, B.B. Mikic, and AT. Patera, "Minimum Dissipation Transport Enhancement by Flow Destabilization: Reynolds[1] Analogy Revisited," J. *Fluid Mech.,* Vol. 192, pp. 365-391, 1988.

[8] N.K. Ghaddar, M. Magen, B.B. Mikic, and AT. Patera, "Numerical Investigation of Incompressible Flow in Grooved Channels. Part 1. Stability and Self-Sustained Oscillations," J. *Fluid Mech.,* Vol. 163, pp. 99-127, 1986.

[9] C.H. Amon and B.B. Mikic, "Flow Pattern and Heat Transfer Enhancement in Self-Sustained Oscillatory Flows," *AIAA* 89-0428, 1989.

[10] C.H. Amon and B.B. Mikic, "Numerical Prediction of Convective Heat Transfer in Self-Sustained Oscillatory Flows," *J. Thermophys. Heat Transt,* Vol. 4, pp. 239-246, 1990.

[11] CT. Leonard, "Mechanical Engineering Issues and Electronic Equipment Reliability: Incurred Costs Without Compensating Benefits," *IEEE Transactions on Components, Hybrids, and Manufacturing Technology,* Vol. 13, No. 4, pp. 895-902, 1990.

[12] AT. Patera, "A Spectral Element Method for Fluid Dynamics: Laminar Flow in a Channel Expansion," J. *Comp. Phys.* Vol. 54, pp. 468-477, 1984.

[13] K.Z. Korczak and AT. Patera, "An Isoparametric Spectral Element Method for Solution of the Navier-Stokes Equations in Complex Geometry," *J. Comput. Phys.,* Vol. 62, pp.361-382, 1986.

[14] S.A. Orszag and LC. Kells, "Transition to Turbulence in Plane Poiseuille and Plane Couette Flows," J. *Fluid Mech.,* Vol. 96, pp. 159-205, 1980.

[15] D. Gottlieb and S.A. Orszag, "Numerical Analysis of Spectral Methods. Theory

and Applications,[11] Vol. 26, CBMS-NSF Monograph SIAM, Philadelphia, 1977.

[16] H. Schlichting, Boundary Layer Theory, New York, McGraw Hill Book Company, pp. 457-465, 1979.

[17] RG. Drazin and W.H. Reid, Hydrodynamic Stability, Cambridge, Cambridge University Press, pp. 153-164, 1981.

[18] C.H. Amon and A.T. Patera, "Numerical Calculation of Stable Three-Dimensional Teritary States in Grooved-Channel Flow," *Phys. Fluids A,* Vol. 1, No. 12, pp. 2005-2009, 1990.

[19] W. E. Pence and J. P. Krusius, "Package Thermal Resistance: Geometrical Effects in Conventional and Hybrid Packages," *IEEE Transactions on Components, Hybrids, and Manufacturing Technology,* Vol. 13, No. 2, pp. 245-251, 1990.

[20] G. L. Lehmann and R.A. Wirtz, "The Effect of Variations in Streamwise Spacing and Length on Convection From Surface Mounted Rectangular Components," in *Heat Transfer in Electronic Equipment - 1985,* ASME-HTD, New York, pp. 39-47, 1985.

[21] R.J. Moffat and A. Ortega, "Direct Air-Cooling of Electronic Components," Advances in Thermal Modeling fif Electronic Components and Systems, Volume 1, ed. A. Bar-Cohen and A. D. Kraus, New York, Hemisphere Publishing Corporation, pp. 129-265, 1988.

[22] E.M. Sparrow, J.E. Niethammer, and A. Chaboki, "Heat Transfer and Pressure Drop Characteristics of Arrays of Rectangular Modules Encountered in Electronic Equipment," *Int. J. of Heat and Mass Transfer,* Vol.25, pp. 961-973, 1982.

Figure Captions

Fig. 1 Grooved-channel geometry characterized by L (periodicity length), a (groove depth), 2h (channel height), and I (separation length).

Fig. 2 Streamlines showing the flow pattern and vortex structure of a steady flow for (a) Groove 1 at R=450, (b) Smount 1 at R=375, (c) Smount 2 at R=375, and (d) Ivtpga at R=375.

Fig. 3 Spectral element mesh for the fluid region showing (a) macro-elemental distribution, and (b) collocation points.

Fig. 4 Sequence of six streamline plots indicating the flow pattern associated with a periodic, self-sustained flow. Flow comes from left to right; (a) Groove 1 at R=780, (b) Smount 1 at R=800, (c) Smount 2 at R=800, and (d) Ivtpga at R=800.

Fig. 5 Streamlines corresponding to (a) Groove 1 at R=780, (b) Groove 2 at R=700, and (c) Groove 3 at R=930.

Fig. 6 (a) Oscillogram and (b) Fourier power spectrum corresponding to a point in Groove 1 at R=780, Groove 2 at R=700, and Groove 3 at R=930, from top to bottom, respectively.

Fig. 7 Isotherms for the (a) steady and (b) oscillatory flows, in Groove 1 at R=450 and 780, Groove 2 at R=450 and 700, and Groove 3 at R=450 and 930, from top to bottom, respectively. The isotherms are normalized, from 0 to 1, and represent equal intervals of temperature.

Fig. 8 Local heat transfer coefficient values versus node number for (a) Groove 1 at R=780 and 450, (b) Groove 2 at R=700 and 450, and (c) Groove 3 at R=930 and 450. The nodal distribution along the surface of the component is displayed in (d).

Fig. 9 Comparison of local heat transfer coefficient values versus node number for all geometries at R=450.

Fig. 10 Local heat transfer coefficient values versus node number for (a) Smount 1 at R=800 and 375 and (b) Smount 2 at R=800 and 375. The nodal distribution along the surface of the component is displayed in (c).

Fig. 11 Local heat transfer coefficient values versus node number for (a) Ivtpga at R=800 and 375. The nodal distribution along the surface of the component

is displayed in (b).

Fig. 12 Spectral element mesh for the sample package (a) macro-elemental distribution, (b) collocation points, and (c) schematic of the major subcomponents.

Fig. 13 Temperature distribution in the sample package using local heat transfer coefficients for Groove 3 at (a) R=930 and (b) R=450; (c) is determined using a spatially-averaged heat transfer coefficient corresponding to Groove 3 at R=930.

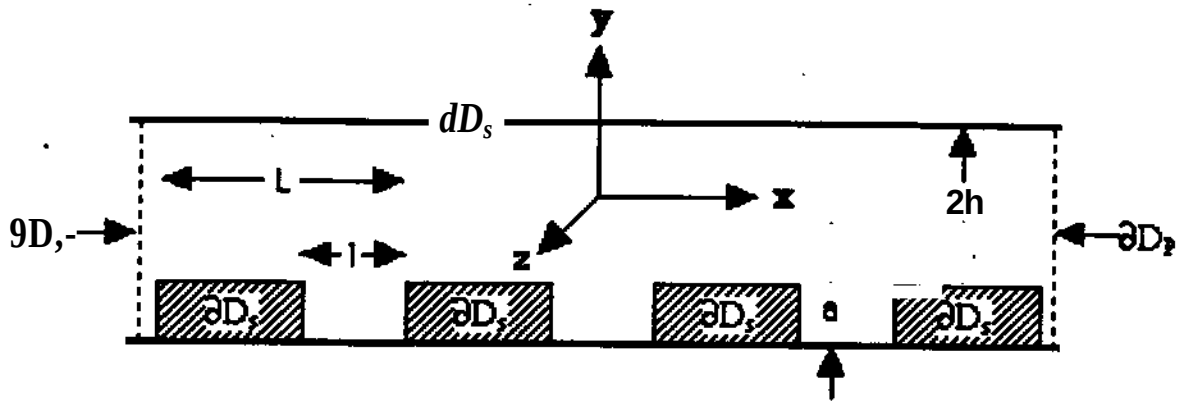

Figure 1

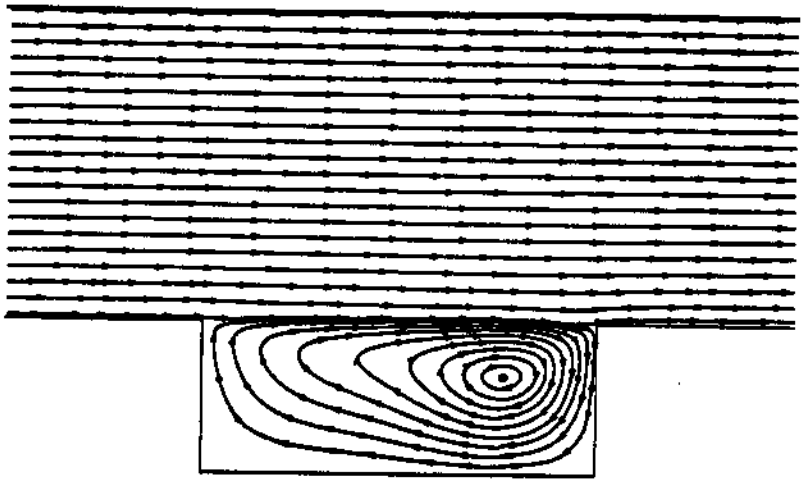

Figure 2a

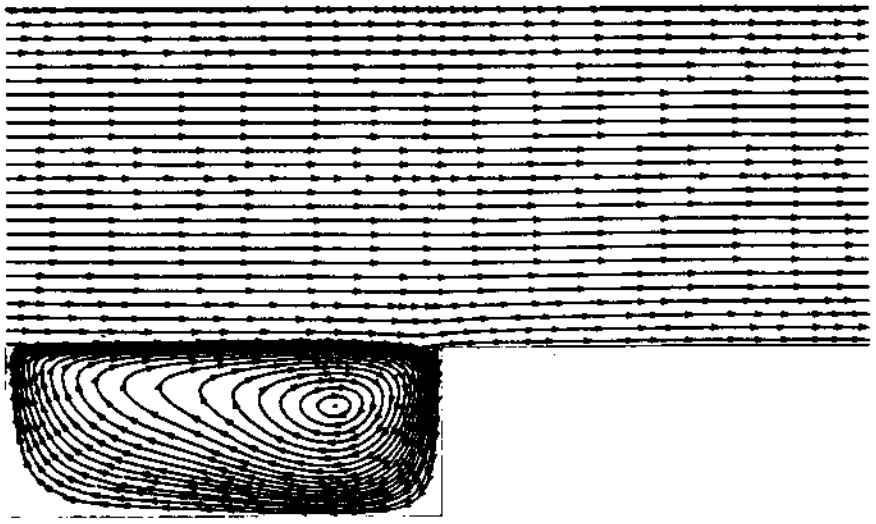

Figure 2b

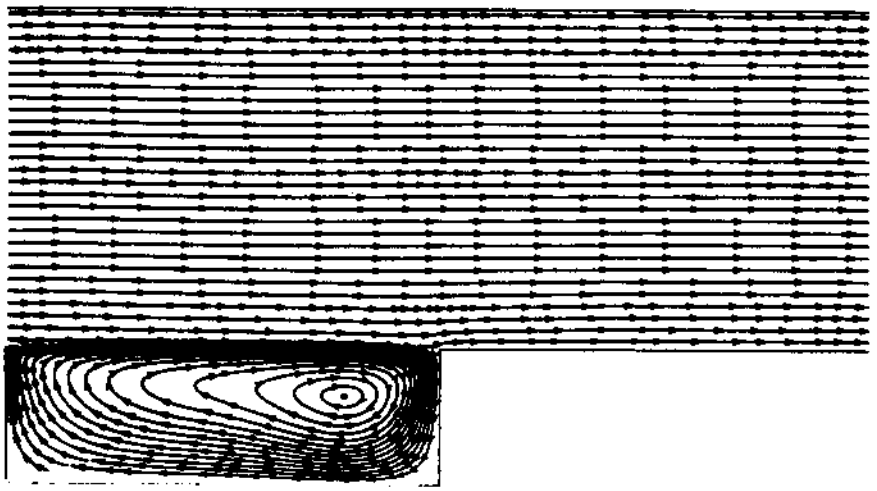

Figure 2c

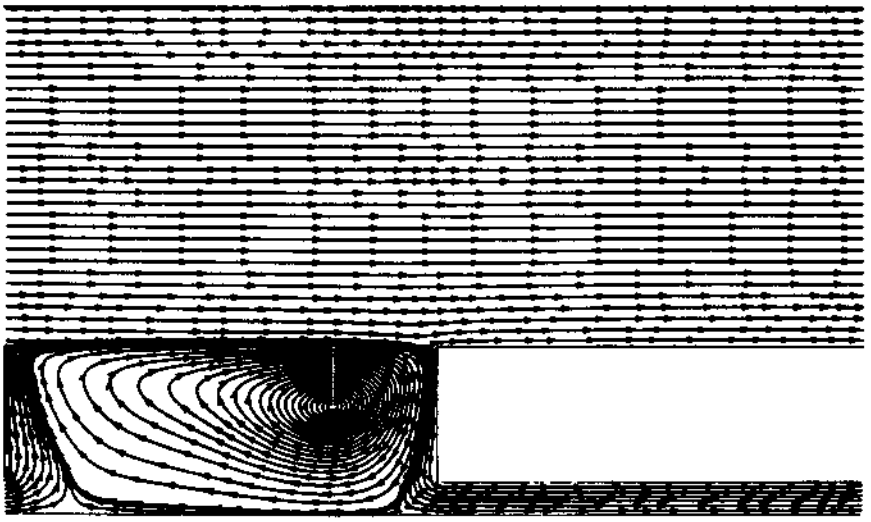

Figure 2d

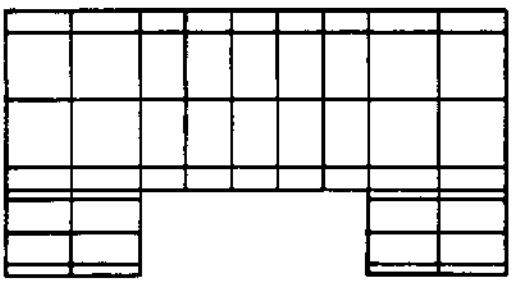

Figure 3a

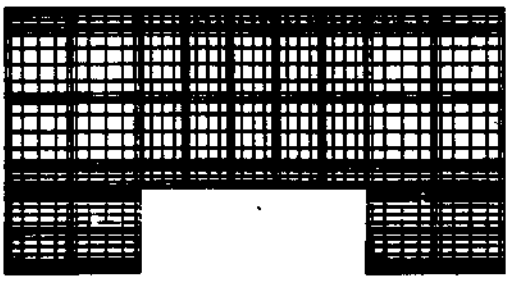

Figure 3b

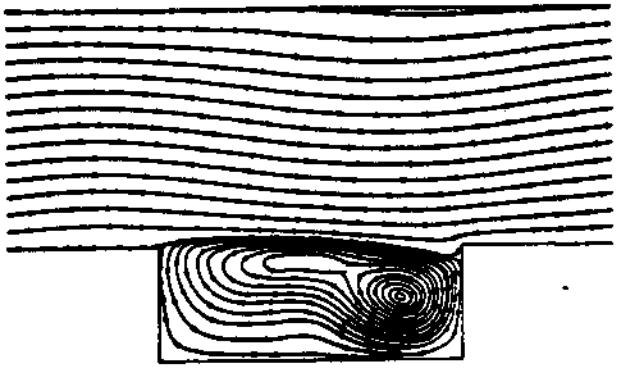

t=0

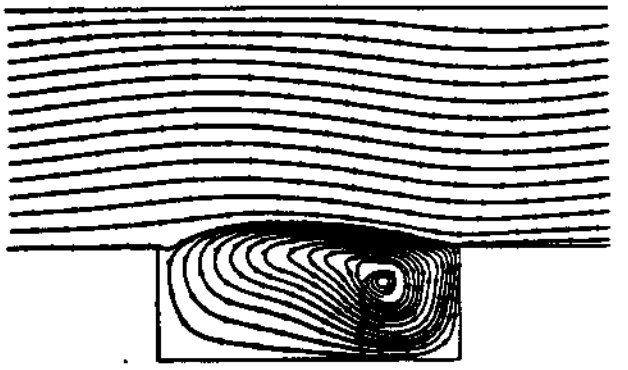

t=Tp/5

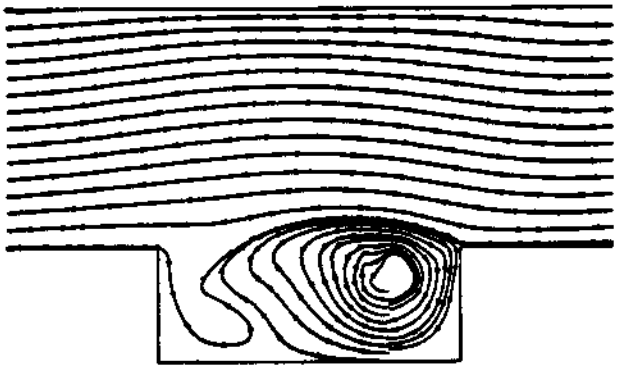

t=2Tp/5

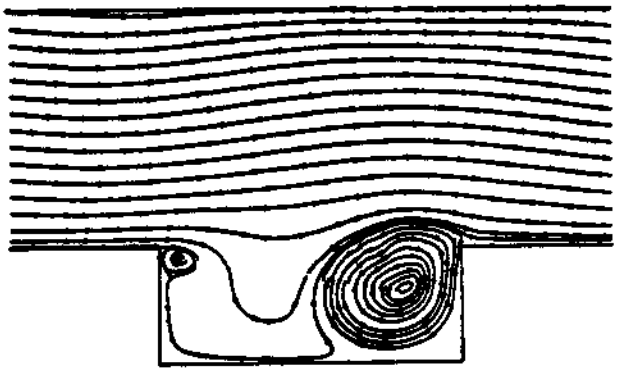

t=3Tp/5

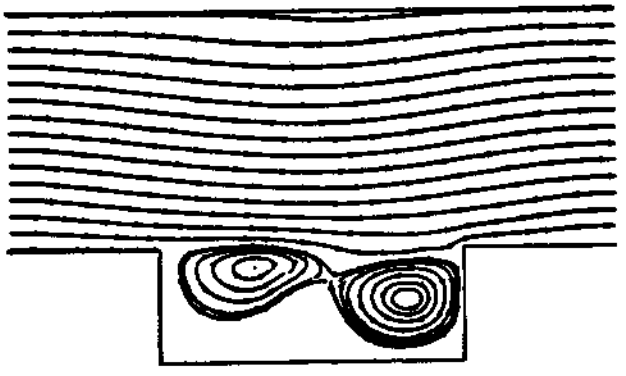

t=4Tp/5

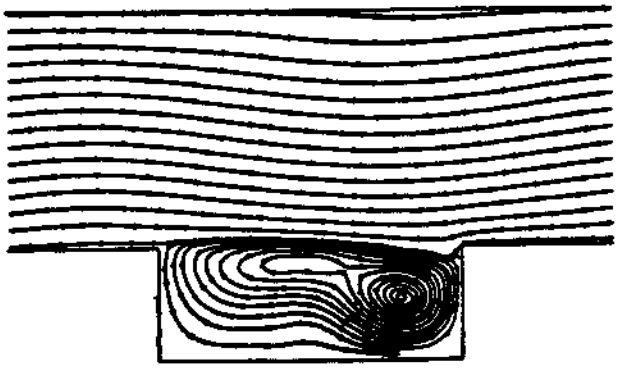

t=Tp

Figure 4a

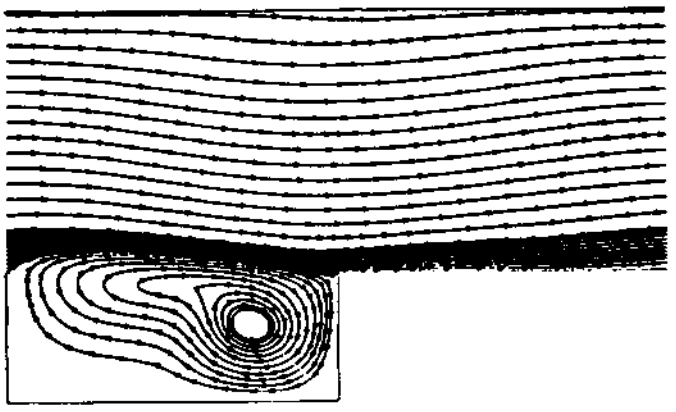

t=0

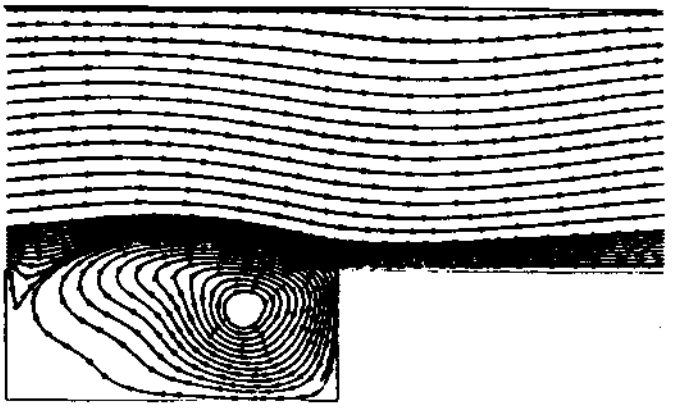

t=2Tp/11

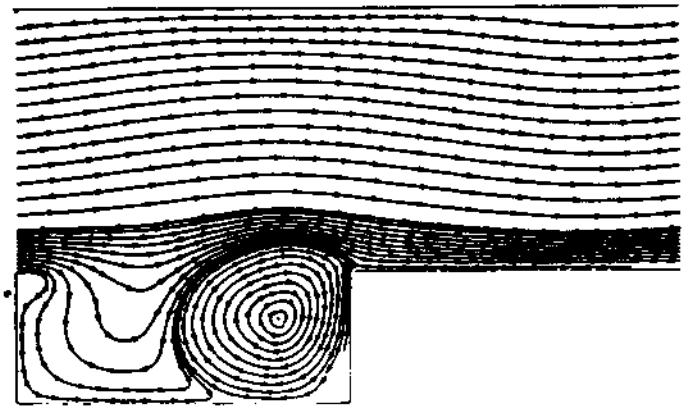

t=4Tp/11

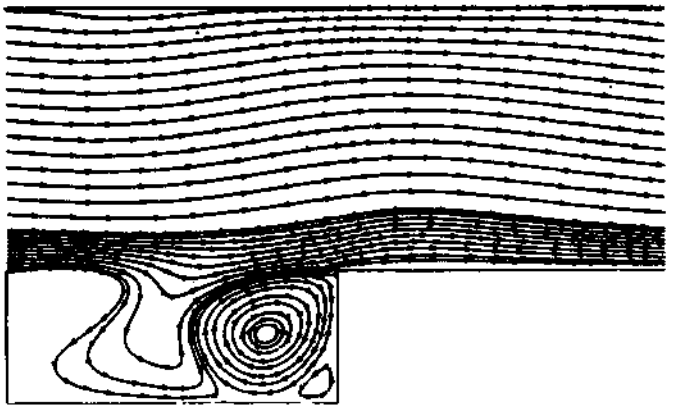

t=7Tp/11

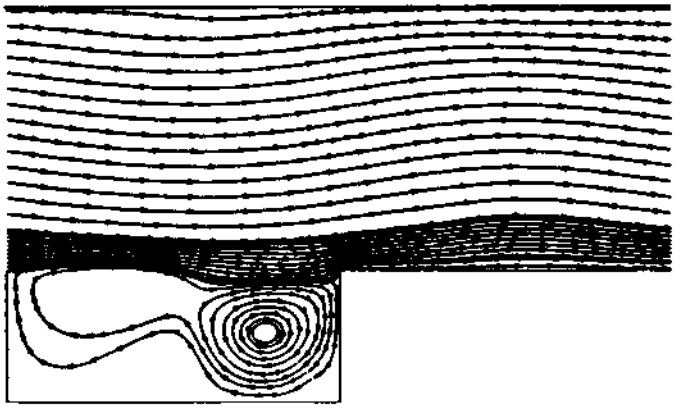

t=9Tp/11

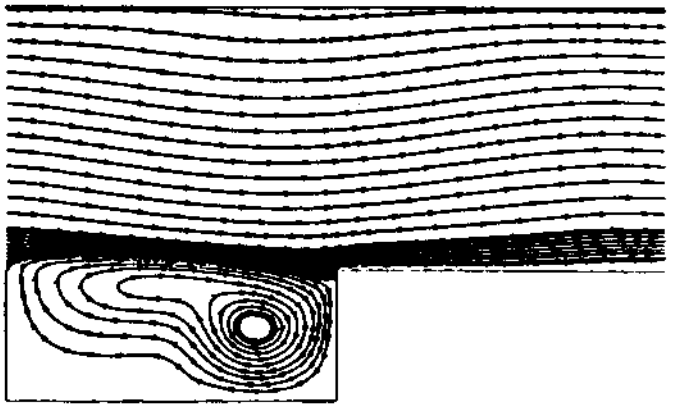

t=T_P

Figure 4b

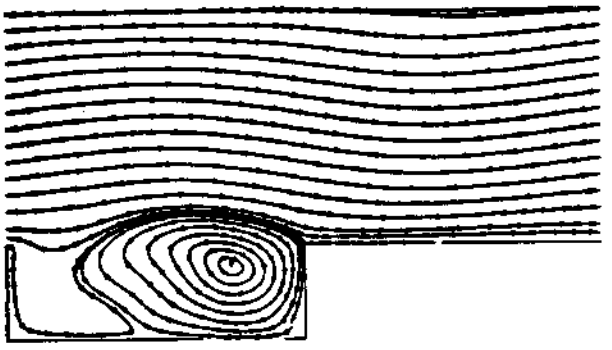

t-0

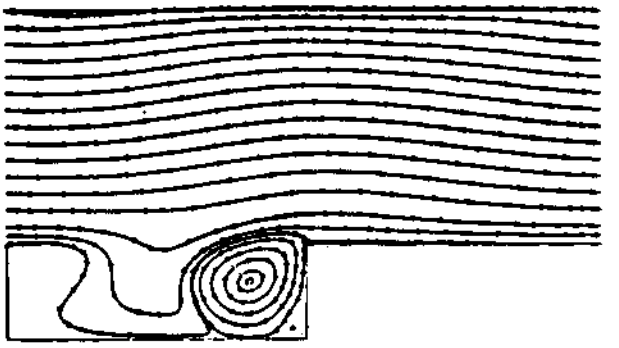

t»7Tp/20

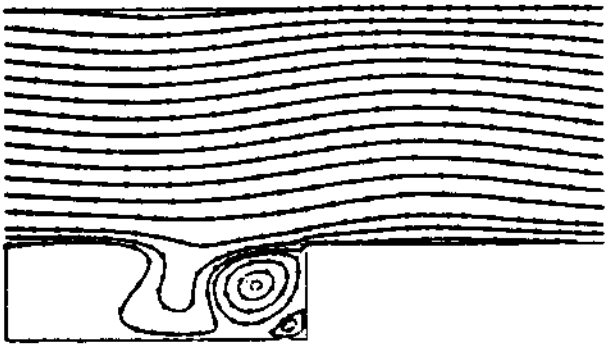

t-10Tp/20

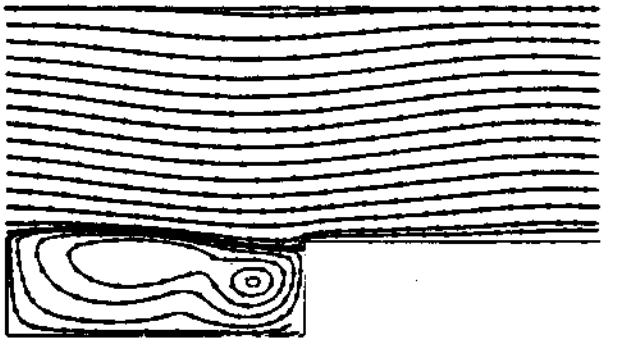

t-14Tp/20

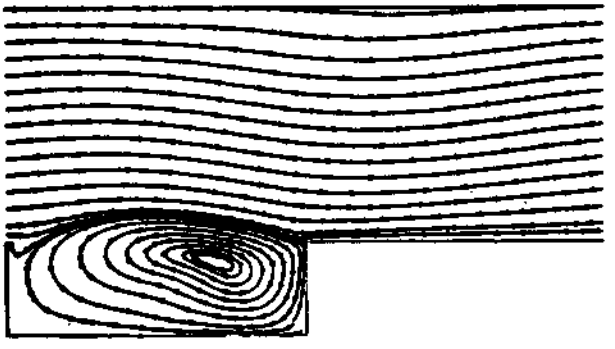

t«18Tp/20

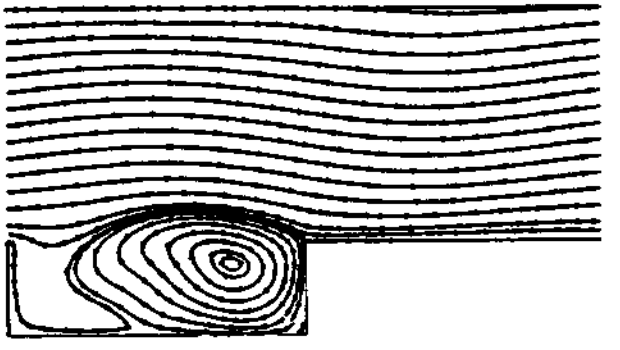

t=Tp

Figure 4c

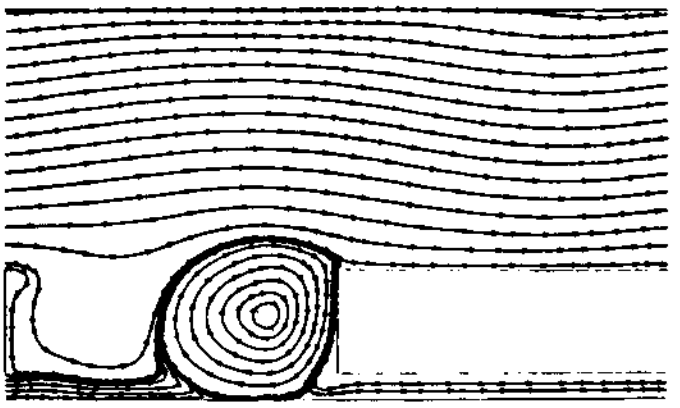

t=0

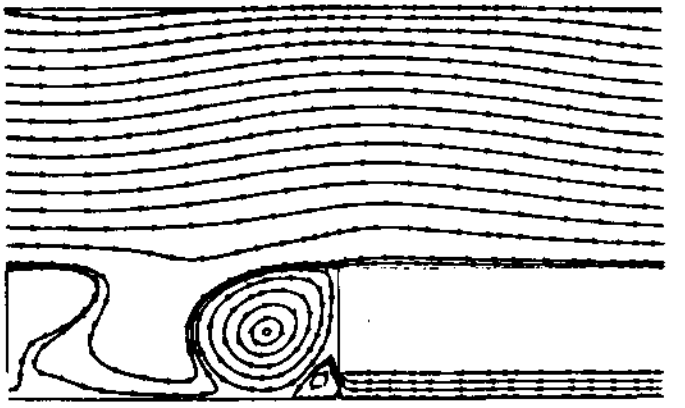

t«5Tp/20

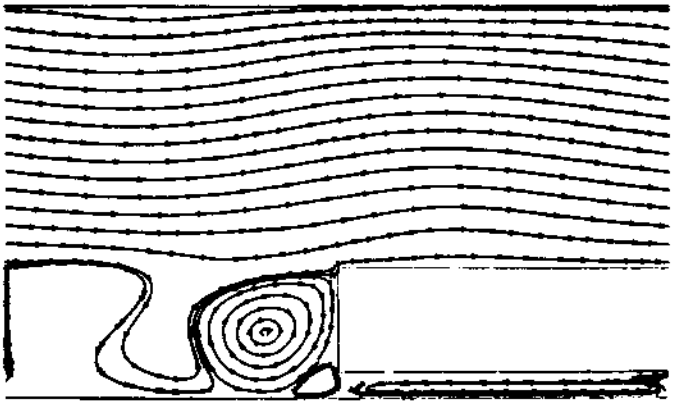

t=7Tp/20

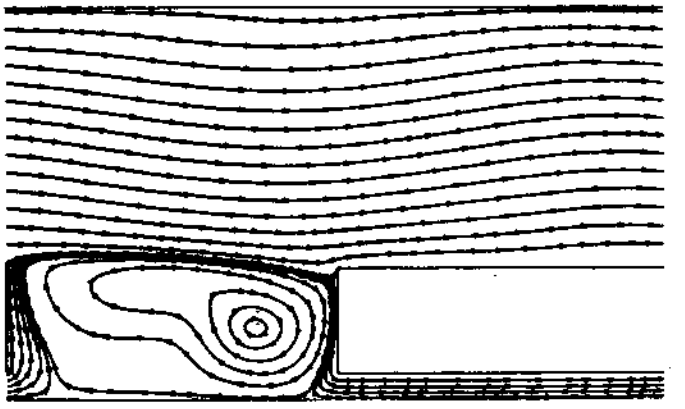

t=12Tp/20

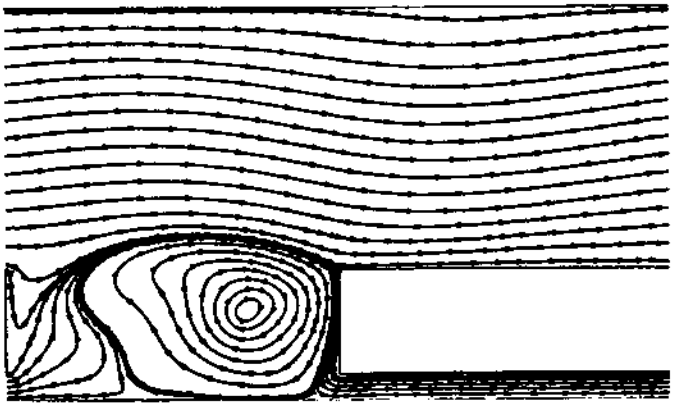

t»17Tp/20

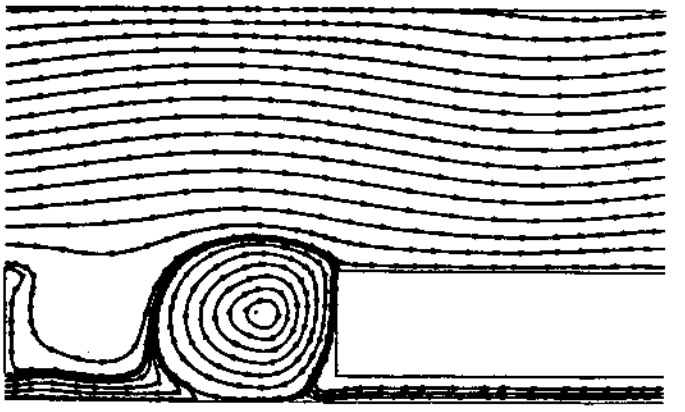

t«Tp

Figure 4d

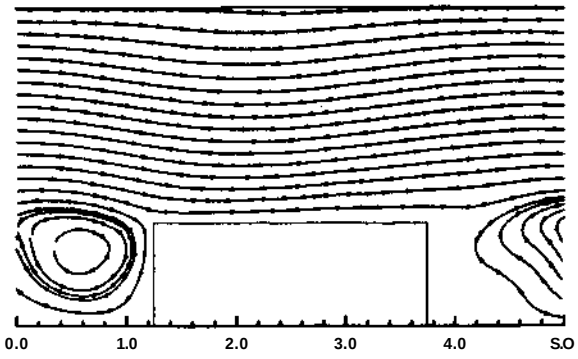

Figure 5a

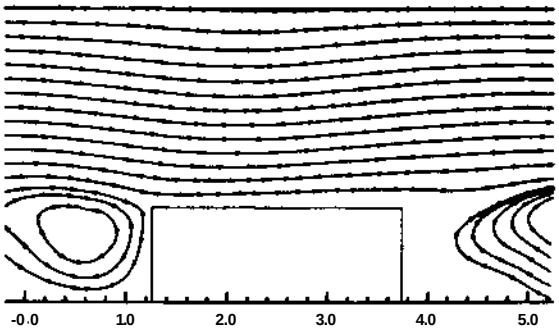

Figure 5b

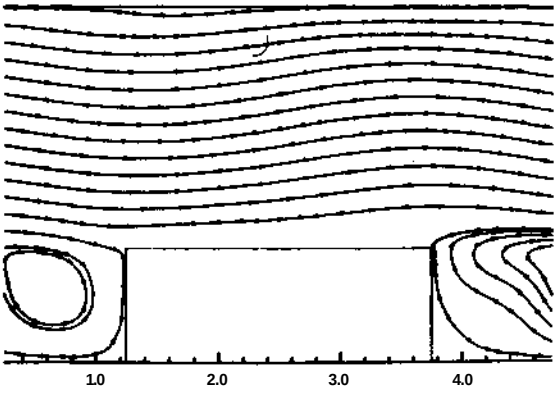

Figure 5c

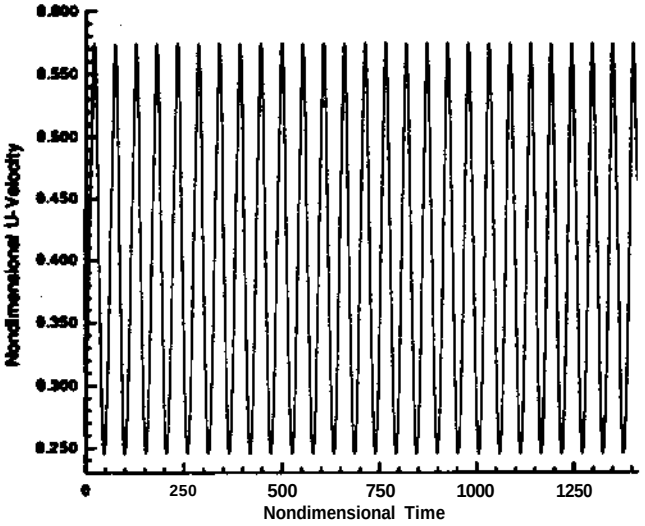

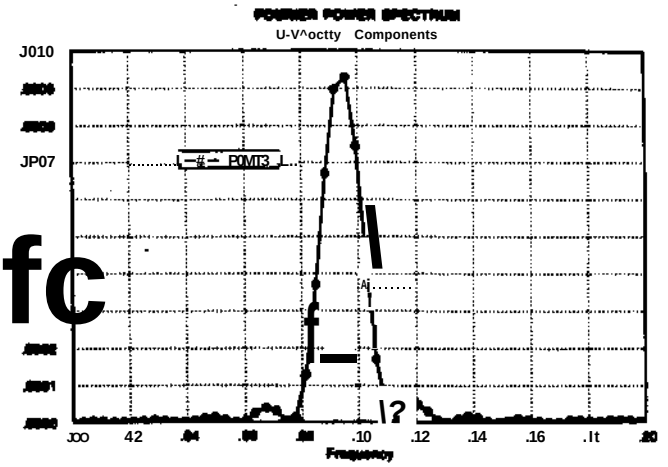

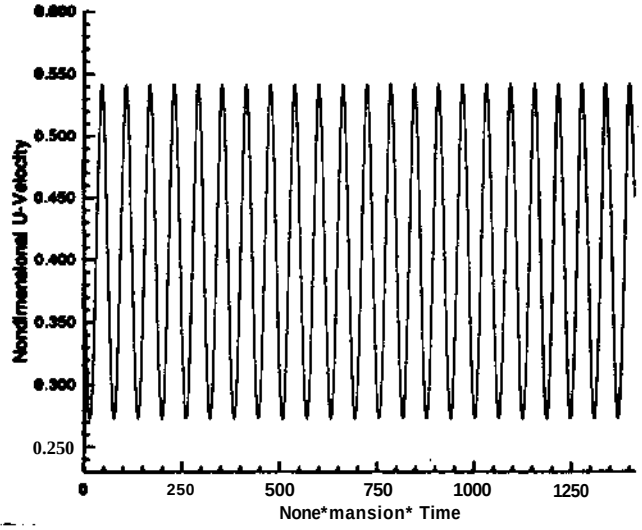

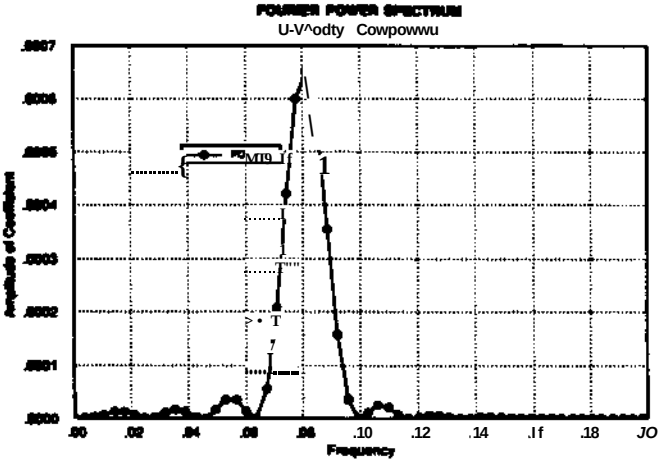

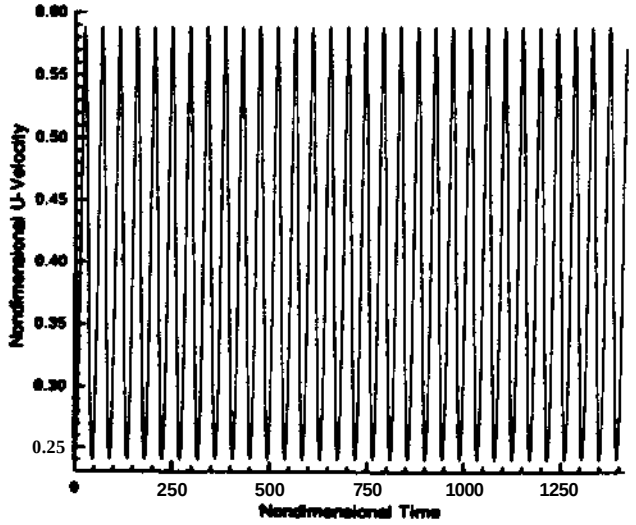

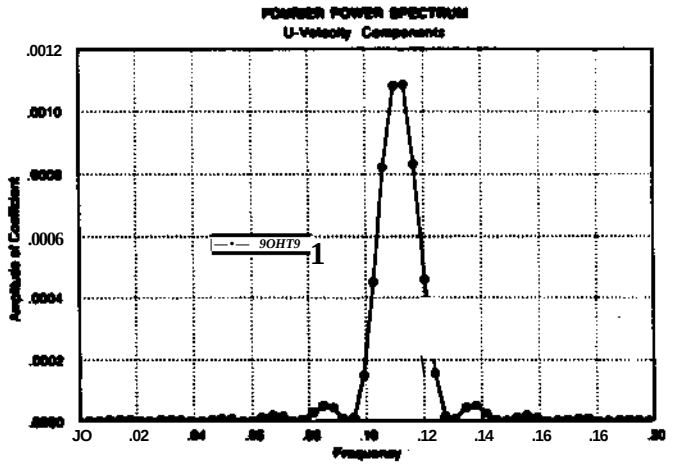

Figure 6a

Figure 6b

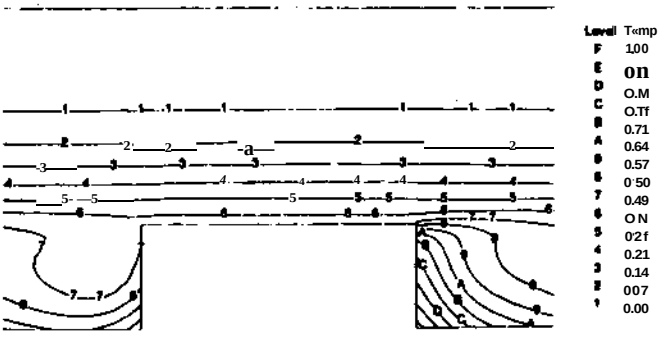

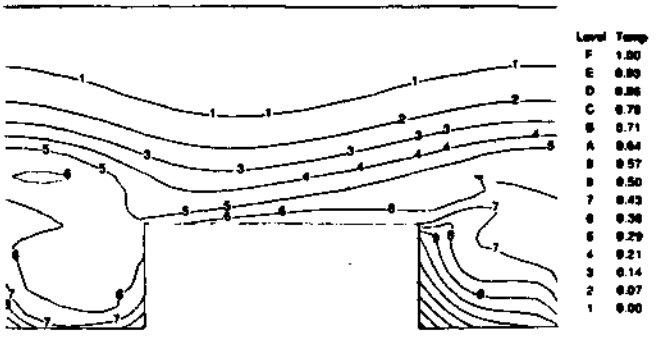

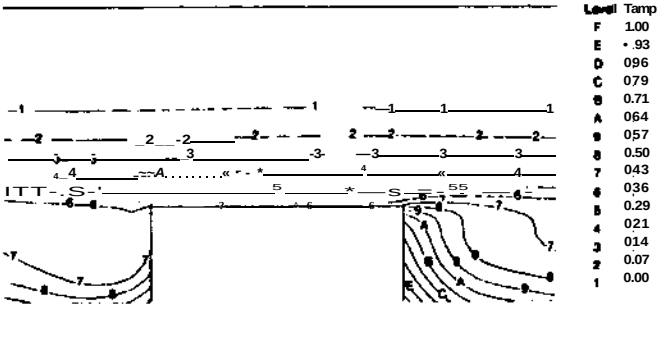

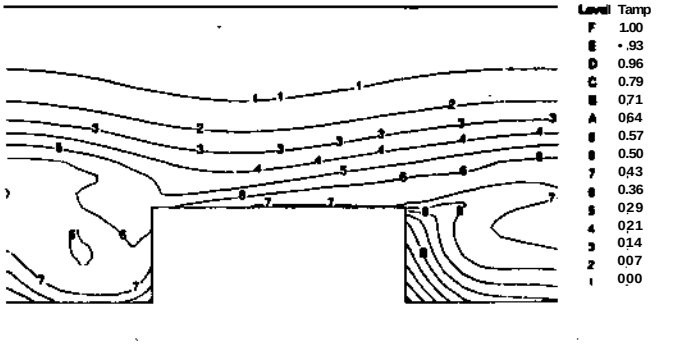

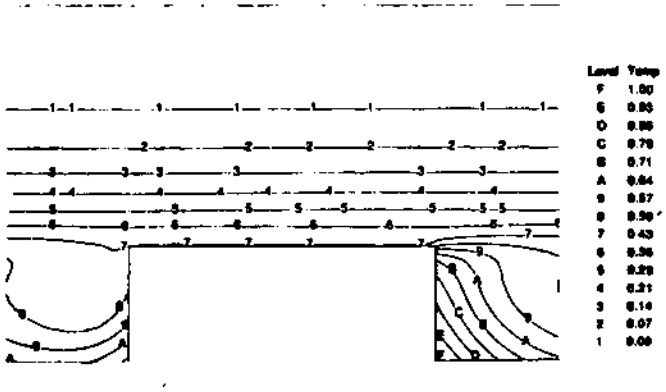

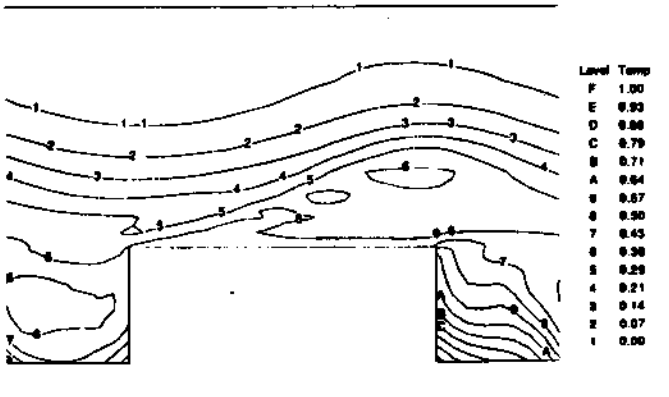

Figure 7a

Figure 7b

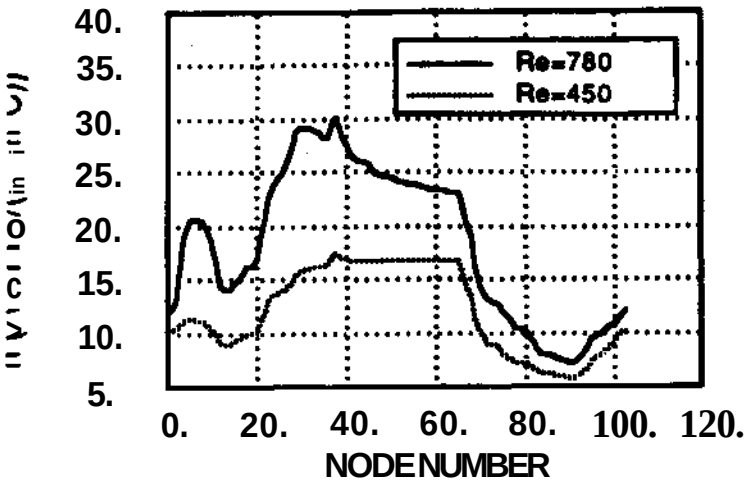

Figure 8a

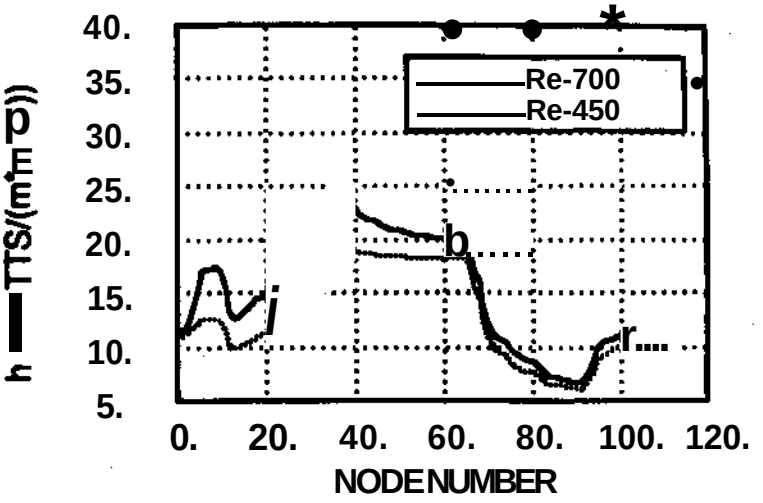

Figure 8b

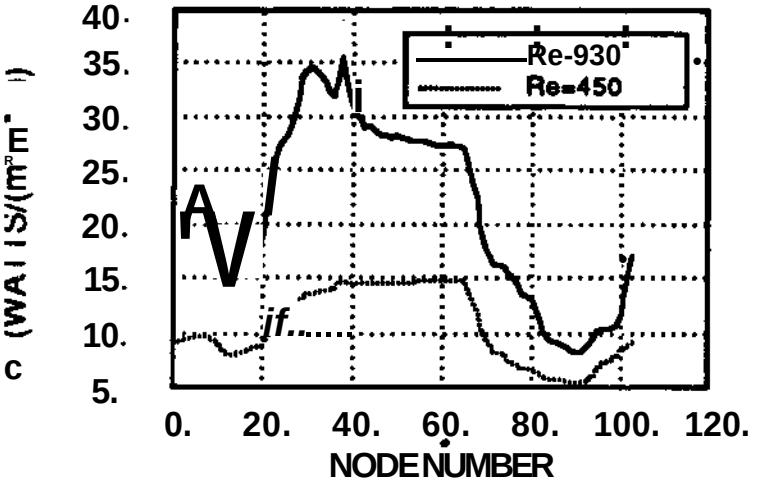

Figure 8c

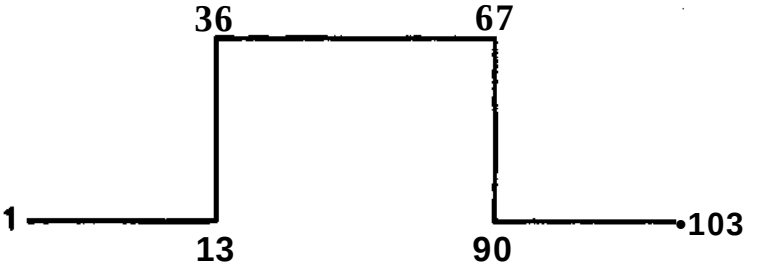

Figure 8d

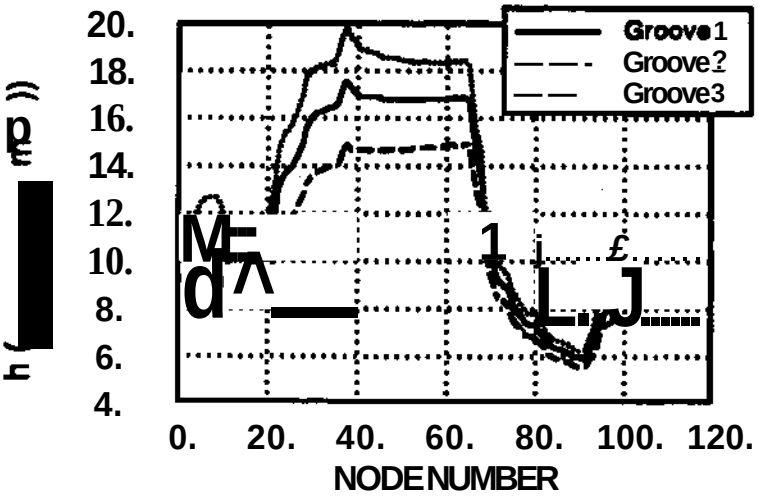

Figure 9

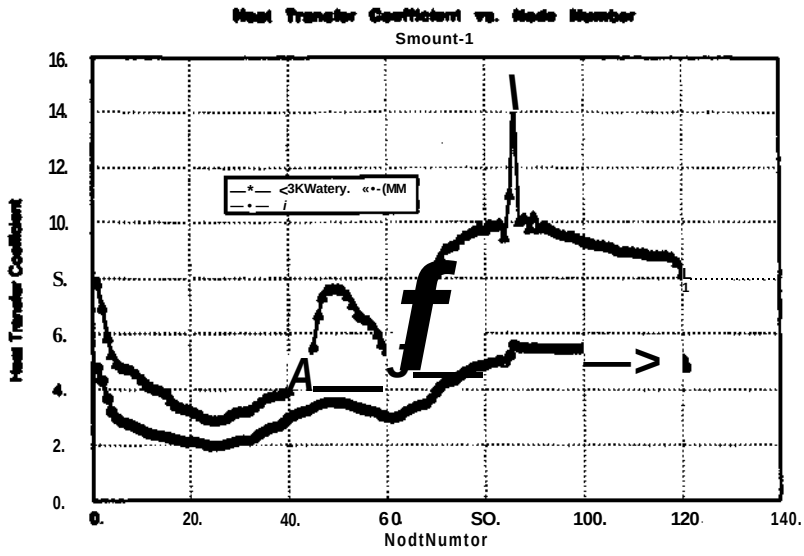

(a)

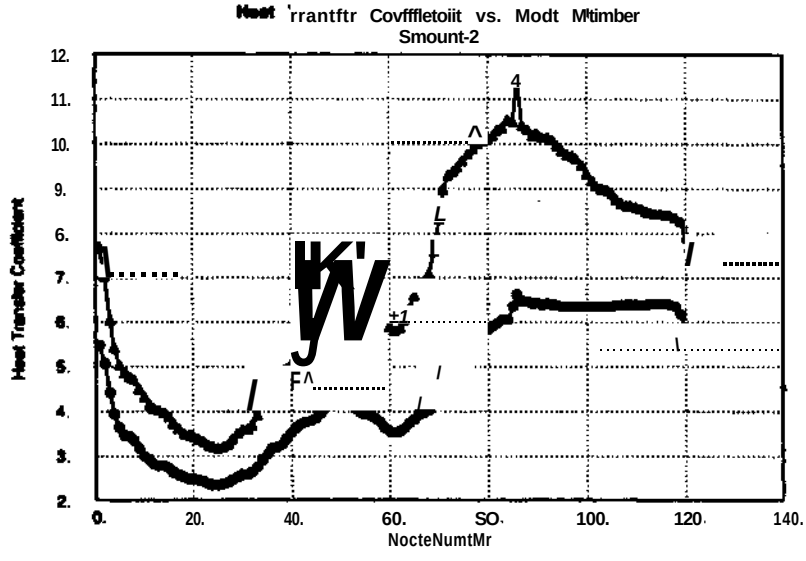

(b)

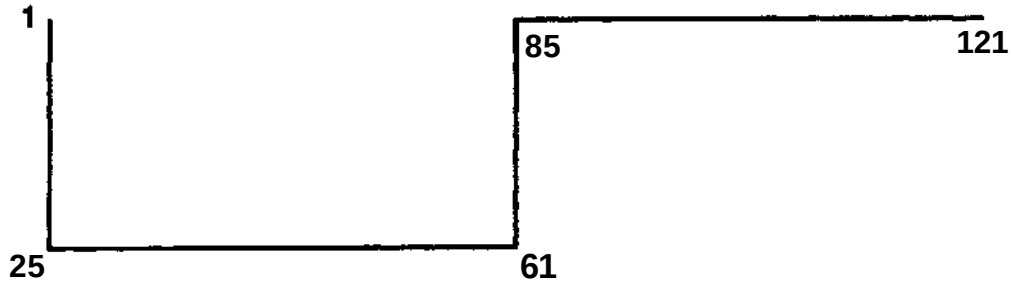

(c)

Figure 10

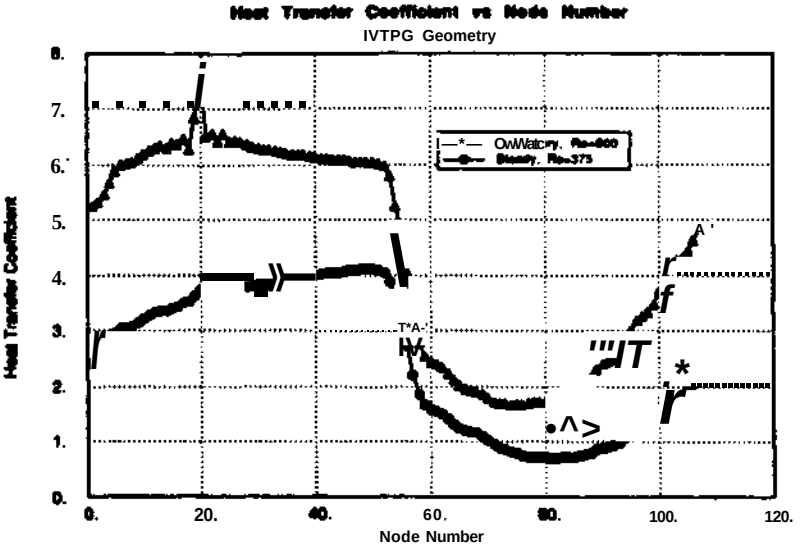
Heat Transfer Coefficient vs Node Number
IVTPG Geometry
Heat Transfer Coefficient
Node Number
0.
20.
40.
60.
80.
100.
120.
1.
2.
3.
4.
5.
6.
7.
8.

(a)

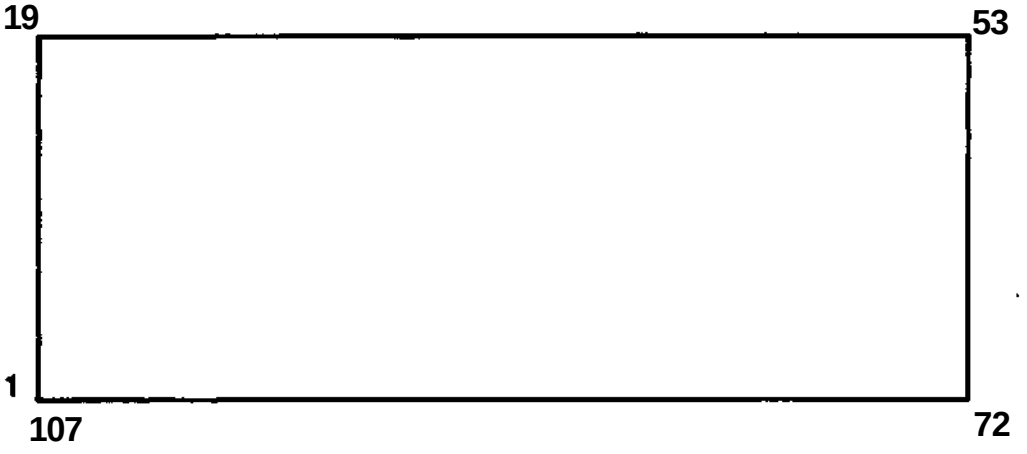
19
53
1
107
72

(b)

Figure 11

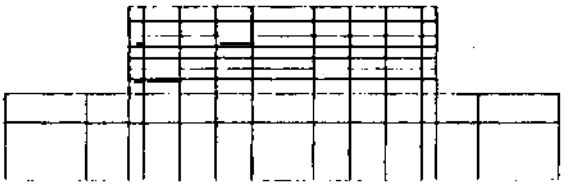

Figure 12a

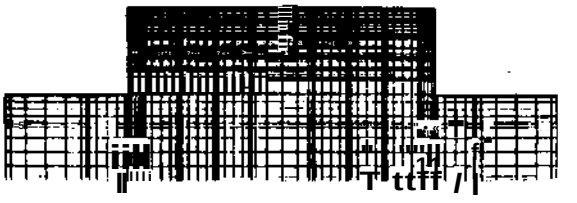

Figure 12b

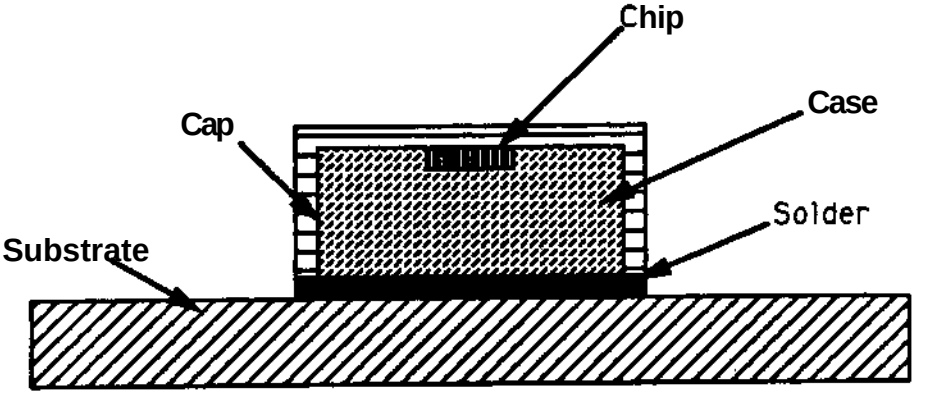

Figure 12c